Asymmetric Contributions to Instantaneous Reserve by Generation, Loads, and Storage

Johannes Heid[1], Walter Schittek[1], Christian Hachmann[1,2], and Martin Braun[1,2]
Wilhelmshöher Allee 73, D–34121 Kassel, Tel. 0561-804-6213
E-Mail: walter.schittek@uni-kassel.de
Internet: http://www.uni-kassel.de/eecs/e2n, http://www.iee.fraunhofer.de
1) Universität Kassel, Fachbereich Elektrotechnik/Informatik, Fachgebiet e²n
2) Fraunhofer IEE, Kassel

Abstract

In the course of decarbonization, interconnected systems will have to be prepared for recurring situations during which they are fed by mostly inverter-based generation. Today, the stabilizing influence of the rotating masses directly coupled to the grid via synchronous generators on every frequency change is essential. The inherent immediate reaction of synchronous generators on voltage-angle changes and frequency variations is called instantaneous reserve. During dynamic situations such as load or generation changes and particularly during the first second after a system split, any active-power imbalance must initially be compensated by instantaneous reserve.

Inherent power-electronic contributions to instantaneous reserve become essential for future situations with abundant renewable feed-in. The generic concept of a virtual synchronous machine (VSM) includes inherent instantaneous reserve but, like for a synchronous machine, the active-power reaction of a VSM is symmetric on positive and negative frequency variations. The immanent characteristics and limitations of possible VSM-coupled grid participants such as photovoltaic plants, storages, charging infrastructure, and different kinds of loads are oftentimes asymmetric in this respect.

This article describes a novel concept of modifications to a generic VSM control scheme enabling asymmetric and even unidirectional contributions to inherent instantaneous reserve. Thus modifying future converters of generators, storages, and different kinds of loads, with an emphasis on charging systems of electric vehicles, can tap potentials unused up to now. Thereby, increased effort (e.g., extra storage, higher ampacity of the semiconductors) for making contributions symmetric can be avoided to a great extent.

Keywords: asymmetric inertia, unidirectional inertia, instantaneous reserve, charging infrastructure, electric vehicle, virtual synchronous machine, synchronous converter.

1 Introduction

The inertia of the synchronously rotating masses of conventional generators (synchronous machines) exerts a stabilizing influence on every frequency change. This behaviour is inherent and occurs without any delay. In a synchronous area, an ongoing frequency decay expresses an

Postprint to 'Tagung Zukünftige Stromnetze 2022', 26-27 Jan 2022, doi:10.17170/kobra-202202015687.
Deutsche Version dieses Artikels: doi:10.17170/kobra-202202015686.

instantaneous active power (P) deficit whereas a rising frequency indicates a P surplus. Corresponding to direction and rapidness of the frequency change, synchronous machines store or discharge kinetic energy and thus temporarily compensate for the instantaneous P imbalance.

The acceleration time constant T_A, a value in seconds used as a measure for the instantaneous reserve realized by a certain synchronous machine relative to its rated active power P_rated, [1] is determined from the moment of inertia J for the angular velocity ω_m of the rotor at nominal frequency [1, p. 10]:

$$T_\mathrm{A} = \frac{J\omega_\mathrm{m}^2}{P_\mathrm{rated}} \tag{1}$$

Considering T_A as well as P_rated of all synchronous machines in a (part of the) grid, the acceleration time constant T_N of the network is a measure for the instantaneous reserve of the (part of the) power system relative to the total demand $P_\mathrm{demand,total}$:

$$T_\mathrm{N} = \frac{\sum(T_{\mathrm{A},i}\,P_{\mathrm{rated},i})}{P_\mathrm{demand,total}} \tag{2}$$

where $T_{\mathrm{A},i}$ and $P_{\mathrm{rated},i}$ are the acceleration time constant and rated power of the ith unit contributing to instantaneous reserve [1, p. 10]. The larger T_N, the more extreme incidents (in terms of relative active-power imbalance) can be tolerated without the resulting RoCoF (rate of change of frequency) exceeding a certain range defined by the transmission system operators, e.g. $-2...+2\,\mathrm{Hz/s}$, cf. [1, p. 3].

Large active-power imbalances occur when cascading line overloads initiate a system split, i.e. the synchronous area is split into two or more parts between which all AC lines remain tripped. The most extreme RoCoF values occur when the disrupted power flows amount to 1/3 or more of the demand in one of the remaining parts, cf. [1]. According to experience, a system split happens every several years for one of the peninsula-shaped peripheral parts of the Continental-European synchronous area, such as Italy or Turkey. Moreover, extreme relative active-power imbalances cannot be excluded to happen (very rarely) for large parts of the synchronous area, namely when a system split goes right through central parts of the interconnected system like it has happened on 4 Nov 2006 in the Continental-European synchronous area.

In the course of decarbonization, interconnected systems will have to be prepared for recurring situations during which they are fed by mostly inverter-based generation. To adequately cope with a system split in such situations, the availability of sufficient instantaneous reserve has to be ensured. The most recent version of the German network development plan [3] specifies an additional need for instantaneous reserve of 600 GWs.

Section 2 exemplarily identifies untapped potentials for asymmetric contributions to instantaneous reserve and puts their possible utilization into context. Section 3 describes constituents of a technical solution by considering the state of the art. Building thereon, Section 4 presents proposed modifications to a generic VSM control scheme. In Section 5, the feasibility of the concept is demonstrated by two case studies of possible implementations. The article closes with Conclusion and Outlook in the Sections 6 and 7.

[1] Relating T_A to P_rated is the pragmatic approach used by, among others, the European transmission system operators [1, p. 10]. A smaller value of T_A for a certain synchronous machine results if T_A is related to the rated apparent power S_rated, and then $T_\mathrm{A} = 2H$, where $H = \frac{1}{2} \cdot \frac{J\omega_\mathrm{m}^2}{S_\mathrm{rated}}$ is the inertia constant expressing the kinetic energy stored in rotating mass relative to S_rated [2, p. 13].

2 Untapped Potentials for Active-Power Variation

The descriptions in this section are based on the assumption that control schemes can be devised that not only tap the potentials for power-electronic contributions to instantaneous reserve but respect the different kinds of obvious limitations. The following considerations stake off fields for research and development that become tangible in view of the technical approach elaborated in the subsequent sections. The considerations correspond to many of the aspects named in the Forschungsroadmap Systemdienstleistungen (research roadmap system services) with respect to instantaneous reserve [4, p. 14 top right + pp. 14f line Momentanreserve].

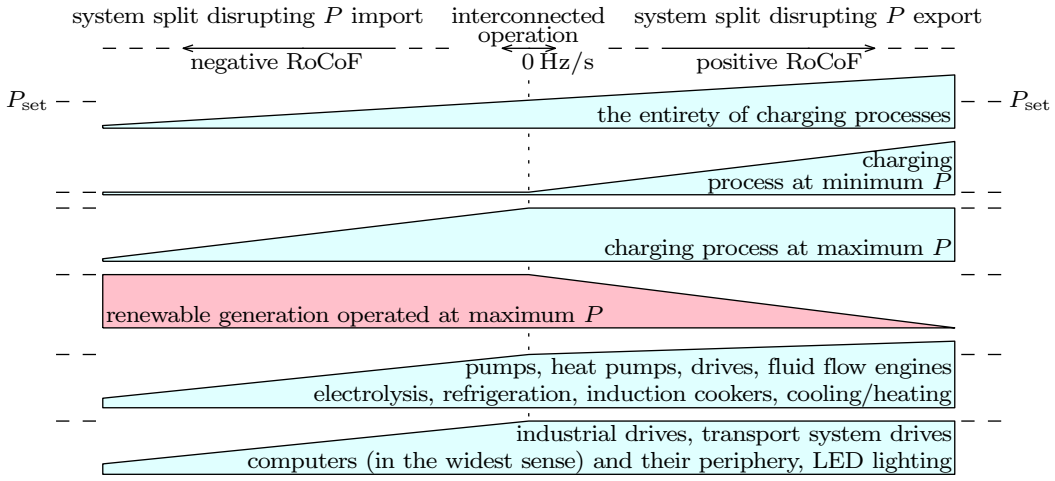

Figure 1: Kinds of non-dedicated units/processes presumably predestined for asymmetric contributions to instantaneous reserve. Lower-hanging fruits placed at the top.

Fig. 1 depicts the assumed potential of power-electronically coupled units for contributions to instantaneous reserve, mostly asymmetric. The lowest-hanging fruits with considerably high potential are charging systems, e.g. for electric vehicles, plug-in hybrids and the like, see Section 2.2.

2.1 Tapping the Potential for Immediate Active-Power Reduction

This subsection looks at the most evident way of participating in instantaneous reserve: The *reduction* of a unit's active-power consumption (for loads) or output (for generation), respectively. This is applicable for all kinds of units/processes shown in Fig. 1, whether they are additionally able to increase their active power – like the charging of an electric vehicle below maximum power – or not.

For inverter-coupled renewable generation, it is state of the art that they are able to reduce their active-power output by up to 100 % within very few seconds in the course of LFSM-O (limited frequency-sensitive mode – over-frequency) [1, p. 15] [5, p. 33]. In rare, extreme cases, e.g. of a short circuit, they must be able to abruptly cut or nullify an arbitrary part of the power inflow, which is oftentimes done via a braking chopper [6]. The remainder of this subsection is about loads, but many of the explanations help further clarify the circumstances of abrupt active-power reductions for feed-in units as well.

For power-electronically coupled loads, it is not state of the art to autonomously react on grid events by (strongly) reducing their active-power inflow for a few seconds and afterwards resuming normal operation. Inherent instantaneous reserve means for loads that the control scheme of the power electronics effectuates variations in the power flowing into the DC link. One constraint is that the controlling components still must get the power they need. And, of course, the DC-link voltage control must not counteract these active-power variations. That means the productive part of the load – the main process – is provided with no more and no less than the currently available amount of DC power according to the active-power variations. It must be ensured that the variations cannot violate the limitations of the load, e.g. the minimum and maximum power of the main process.

Even for long-living electro-mechanical equipment, an extreme active-power reduction after a severe system split will not happen more than a very few times during lifetime, if at all. Undergoing an abrupt strong function impairment is only admissible for kinds of loads where function impairment does not induce more than slight cost or even endanger persons. Consequently, no participation in instantaneous reserve is admissible for loads like 3D printers, milling machines running in finish mode, traffic lights and moving stairways. However, on closer examination it becomes clear that even passenger elevators and ropeways, as well as LED lighting switched off via timing, are, in principle, suitable for participating in inherent instantaneous reserve. Kinds of devices (other than charging processes, cooling and heating) where a short function impairment might be perceived by users ought to have an information channel (display, message app) by which the user is informed immediately not to deem the device defective.

More and more loads have an electronic main process, i.e. their instantaneous active-power consumption fluctuates with the workload of a CPU (central processing unit) or is highly controlled by a CPU. Those devices such as computers without UPS (uninterruptible power supply), information displays, monitors or other computer periphery are equipped with energy-saving mechanisms for times of low workload or inactivity. These mechanisms could be enhanced and/or redesigned for being able to follow the AC-side active-power reductions on DC side in real time, coordinated by the CPU that governs the control of the power supply.

During interconnected operation, e.g. in the Continental-European synchronous area, there is an incessant demand for instantaneous reserve, however, the actually deployed active power can be expected to fluctuate at very low levels over years compared to the maximum active-power variation the individual unit would be able to deploy. The following attributions of DC-side effects to instantaneous-reserve reactions on AC-side events are purely qualitative; actual active-power values and times will depend on the kind of DC-side load and the characteristics of the converter.

a) Continuous frequency movements (every day): To be covered by the DC voltage link of the power electronics for large parts of time, without affecting the DC-side load. [2]
b) Larger frequency fluctuations (several times a week): Slight short-time reductions of the DC-side power can be assumed to remain unnoticeable on most kinds of main processes;

[2]The energy deviation in the DC link is proportional to the frequency deviation if the DC link provides the active power for instantaneous reserve with a constant T_A value [7, p. 4], cf. [8, pp. 2f].

background functions slowed down.

c) Very large contingencies (a few times per year): Function of DC-side main process slowed down but not impaired or aborted; no damages or cost; automatic entry into system log: 'extraordinary AC power fluctuation'.

d) System split with high percentage of active-power imbalance (once in several years): Short-time loss of function with no or justifiable collateral damage.

Whereas charging systems and other more or less flexible loads can (at least slightly) also increase their active-power consumption (see next subsection), many kinds of units are not able to do so but nevertheless to strongly contribute to instantaneous reserve.

Photovoltaic (PV) as well as wind generators often feed in their instantaneous technical maximum power. They are always able to reduce their feed-in to any adequate value in the range 100...0 % during a frequency increase.

However, on occurrence of a frequency decay, those power-electronically coupled loads appropriately take the complementary role (in the sense of [4, p. 14 upper right, b)]) that are able to (in an extreme case) strongly reduce their instantaneous active power.

Examples for kinds of loads predestined for such unidirectional instantaneous reserve are, cf. lowest unit in Fig. 1, fast chargers for electric vehicles, chargers for trucks via overhead line, milling plant, transport-system drive, LED lighting (cf. [8]), industrial drives with speed control such as drilling, grinding, and milling machines; the latter only in rough mode, if applicable. Furthermore loads with an electronic main process, such as computers (in the widest sense) and their periphery, as addressed above. Besides, for some loads mentioned in the next subsection temporary or permanent reasons might apply not to increase their active-power consumption.

2.2 Charging Processes

Concepts where storages start charging or discharging in the moment when instantaneous-reserve power is needed are not in focus of this article. This is emphasized by using the notion (running) 'charging processes'. The prime example for such kind of contribution to instantaneous reserve is the charging of all kinds of electric vehicles [9].

How much a charging process can decrease and increase its active-power consumption depends on the working point. The possibility to increase may be several times as large as the possibility to decrease, or vice versa. In most cases, T_A needs to be changed with the RoCoF direction or to be set to zero in one direction.

Apart from the charging of batteries, charging processes in the wider sense are characterized by some kind of storage that is being filled at some average throughput. The throughput can be tolerated to undergo abrupt decreases and increases, the admissible strength thereof depending on the technology and the working point. That can be utilized for contributions to instantaneous reserve.

Examples for devices performing charging processes of chemical, gravitational-potential, kinetic or thermal 'storages' are, cf. 5^{th} unit in Fig. 1, electrolyser with self-commutated converter, pump storage in pump mode, many kinds of drives, pumps and fluid flow engines, heat

pumps [10], air conditioning (cf. [11]), refrigeration with inverter (cf. [12]), induction cookers (private and commercial), microwave ovens. It is not far-fetched to assume that the contributions of all 'charging processes' to instantaneous reserve in both directions will prove to be rarely equally strong but mostly of similar order of magnitude.

3 Constituents of a Technical Solution

3.1 Instantaneous Reserve by Virtual Synchronous Machines

A 4-quadrant voltage-source inverter with a control scheme enabling it to behave electrically as if it had synchronously rotating mass [13, pp. 18f] is called *grid forming* or in German *spannungseinprägend* (voltage impressing). In research, such inverters are proposed for feed-in [14] [15], storage [16] [9], and special kinds of loads equipped with a 4-quadrant inverter [17] [18], e.g., for reactive-power control. Beside the use of the mentioned adjectives, the notion 'synchronous converter' (German: Synchronstromrichter) has been brought up in project meetings of the German project Netzregelung 2.0 (cf. Section 8) as a generic term, analogous to synchronous machine. Whereas the mentioned adjectives stipulate the ability of acting as an AC voltage source, a synchronous converter might also well be rectifier hardware (e.g. Vienna Rectifier [19] [20] [21]) hosting a control scheme for inherent instantaneous reserve. An important part of the power-electronically coupled kinds of units considered in Section 2 are three-phase or single-phase [9] loads.

'Virtual synchronous machine' (VSM) [22, pp. 10f] [23] is one category of control schemes realized by software that can be used to design synchronous converters based on state-of-the-art converter hardware. Another one is 'SelfSync' [22, pp. 5ff]. VSM control schemes let feed-in inverters as well as power-electronically connected loads (e.g. with Vienna Rectifier [21]) and storage contribute inherent instantaneous reserve.

The key elements of a VSM control, see Fig. 2, are

- the virtual AC voltage source $\underline{V}_{\text{virt}}$, equipped with emulated inherent inertia and maintaining its own frequency f_{virt}, voltage angle, and amplitude,
- the virtual impedance $\underline{Z}_{\text{virt}}=R_{\text{virt}}+jX_{\text{virt}}$ establishing a significant voltage-angle difference between $\underline{V}_{\text{virt}}$ and the PWM voltage $\underline{V}_{\text{PWM}}$ (pulse width modulation).

The active-power imbalance is

$$\Delta P = P_{\text{set}} - P_{\text{meas}} \tag{3}$$

with P_{set} being the active-power setpoint. In this article, a positive sign of ΔP always indicates

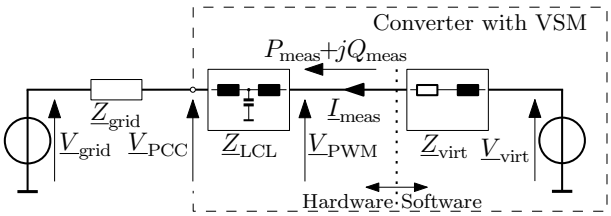

Figure 2: Principle of a VSM, universally applicable to generators and loads (one-phase equivalent circuit, generator view of the converter)

a positive active-power imbalance, resulting in a positive acceleration of f_{virt}. Fig. 2 adopts the generator view but can easily be interpreted for a load converter as well. P_{set} and P_{meas} have negative values then, and f_{virt} accelerates if $|P_{\mathrm{meas}}|>|P_{\mathrm{set}}|$.

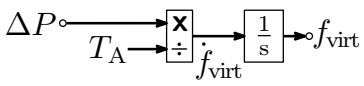

Figure 3: Frequency-adaption mechanism of a VSM, to be understood in p.u. quantities (per unit)

The instantaneous frequency and RoCoF gaugeable in the grid dynamically differ from f_{virt} and $\dot{f}_{\mathrm{virt}}$ of $\underline{V}_{\mathrm{virt}}$ in the VSM, see Fig. 3. f_{virt} is the output of an integrator, consequently $\dot{f}_{\mathrm{virt}}$ is its input. Determined from continuous active-power measurement, $\dot{f}_{\mathrm{virt}}$ in Hz/s is calculated as:

$$\dot{f}_{\mathrm{virt}} = \frac{\Delta P}{P_{\mathrm{rated}}} \cdot \frac{f_{\mathrm{rated}}}{T_{\mathrm{A}}} \tag{4}$$

When the voltage angle of $\underline{V}_{\mathrm{PCC}}$ (point of common coupling) changes, e.g. at the beginning of a frequency variation, the power flow P_{meas} through $\underline{Z}_{\mathrm{virt}}$ changes accordingly. On occurrence of a negative RoCoF, a feed-in VSM inherently acts towards increasing its $|P_{\mathrm{meas}}|$ whereas a load VSM acts towards decreasing its $|P_{\mathrm{meas}}|$. For a positive RoCoF, it's vice versa.

Throughout this article, beside synchronous converters of storages only those synchronous converters of feed-in units or power-electronically coupled loads are of interest that do not have access to some kind of storage and do not restrict their contributions to instantaneous reserve to energy variations in the DC-link capacitor. On occurrence of strong frequency movements, those units will experience variations of the instantaneous active power associated with their main purpose, cf. Section 2. Every unit (feed-in, load, storage) has active-power limits that must be taken into account when deciding about the control reserves, a positive and a negative P value. Based on eq. (4), T_{A} can be calculated as:

$$T_{\mathrm{A}} = \frac{|\Delta P_{\mathrm{max}}|}{P_{\mathrm{rated}}} \cdot \frac{f_{\mathrm{rated}}}{|\dot{f}_{\mathrm{virt,max}}|} \tag{5}$$

$\dot{f}_{\mathrm{virt,max}}$ is the strongest expected RoCoF in the grid. ΔP_{max} is the active-power reserve available for instantaneous reserve; since a standard VSM can only have one uniform T_{A}, $|\Delta P_{\mathrm{max}}|$ must represent the weaker of the two reserves. In case of a RoCoF beyond $|\dot{f}_{\mathrm{virt,max}}|$, the active-power variation of the synchronous converter needs to be actively limited.

3.2 Asymmetric VSM Operation

Many kinds of feed-in units and loads would be able to easily and quickly reduce their active power but not or only with significant effort to increase it, cf. [24, S. 67ff]. Consequently, a large control reserve leading to a large T_{A} ought to be allotted for one RoCoF direction and – if additional effort and cost is to be avoided – only a small or no control reserve for the other, leading to a small T_{A} or to $T_{\mathrm{A}} = 0$ according to eq. (5). Consequences in the face of Fig. 3 are considered and solved in Section 4.

Standard VSM control schemes do not support asymmetric contributions to instantaneous reserve, i.e. differing T_{A} values for the two RoCoF directions. Therefore, only uniform small

control reserves can be used where limitations are asymmetric. This would possibly leave most of technically available reserves unused. It is far from trivial to modify a standard VSM control scheme in order to respect asymmetric control reserves where one of the complementary reserves is only a very small fraction of the other or to realize $T_A = 0$ for one RoCoF direction.

In Section 4, a technical approach is described that allows for asymmetric VSM operation. The term 'virtual synchronous machine' in its narrower sense is no longer applicable to the control schemes governing such an asymmetrically-acting converter, because its behaviour does no longer follow any of the synchronous-machine models being used for VSMs. The generic term 'synchronous converter', see Section 3.1, still applies. Nevertheless, the term VSM is still used in this article, implying that at the core of the synchronous converter a VSM in the narrower sense is working, which is actually correct for the described approach: The modifications of the VSM control scheme encapsulate the core VSM control scheme.

3.3 State of Research

During the last years, many researchers have developed enhancements to basic VSM principles. The approach described in this article can be characterized by the following aims and mechanisms:

1. It aims at a dynamic adaption of the emulated inertia, i.e. of T_A.
2. It aims at respecting power limits of the process(es) connected to the DC link without using an additional storage.
3. It uses a manipulation of the basic ΔP calculation eq. (3).
4. It uses a dynamic adaption of the virtual impedance $\underline{Z}_{\text{virt}}$ in Fig. 2.

There are publications aiming at improvements similar to those described in this article and/or using similar or the same mechanisms. Individual publications investigate no more than one or two of the above-mentioned four aspects.

1. The **dynamic adaption of the emulated inertia**, with the aim of increasing transient stability, can be found in literature starting with [25] and [26], where the moment of inertia J is changed between a large and a small value, based on the deviation from the nominal frequency and the derivation of the frequency of the machine. In subsequent research, this so-called interval-based approach [27] is modified with respect to damping [28] [29] [14] [27], to small-signal stability [30], to initial synchronization [31], to thresholds for adaption [32], and to following the centre-of-inertia frequency [33]. Another approach using a dynamic adaption of inertia aims at a sufficient stability margin by applying online grid-impedance measurement [34]. Further approaches using dynamic adaptions of inertia and damping aim at containing the control effort by applying a linear quadratic regulator [35] [36] or address the performance during different dynamic situations [37] [38] [39]. Another approach [40] uses dynamic adaptions of inertia and $Q(U)$ droop for improving the voltage stability.
2. For **respecting power limits** while operating a VSM, different approaches can be found in literature. In [41], a PV plant is operated below the maximum power point (MPP) in order

to be able to follow negative RoCoFs. In [42], the energy for participating in instantaneous reserve is taken out of the central DC-link capacitor of a hybrid AC/DC grid. In order to keep the capacitor voltage within limits of normal operation, the inertia is dynamically adjusted, and the principle of adjustment leads to very small inertia in the course of extreme contingencies.

3. A **manipulation of the basic ΔP calculation** is used for different purposes in many publications. For implementing a consensus-based contribution to frequency restoration, an integral of ΔP is negatively fed back into the ΔP calculation in [43] with its follow-up [44] and also in [45]. For limiting the inverter current during short circuit, the P setpoint in [46] respectively the measured P in [47] get adapted values during low terminal voltage. For shaping the active-power output during transients, a fraction of $\mathrm{d}P/\mathrm{d}t$ is added to ΔP in [48]. For shaping the transient performance, a feedback value is added to the result of the ΔP calculation as part of a novel control method proposed in [49] together with [50]. For implementing a nonlinear adaptive robust control strategy, ΔP is modified in [15] by values calculated from the frequency and rotor angle. For stabilizing transient behaviour, a sign change of ΔP is invoked in [51] under certain circumstances. For improving transient stability, ΔP is modified in [52] by an additional power term and auxiliary inertia. For improving small-signal stability, ΔP is modified in [53] by a frequency and a power feedback. For continually restoring a short-term storage to the desired state of charge, [54] manipulates the ΔP calculation.
4. A **dynamic adaption of the virtual impedance** is used in literature for different purposes. [55], [56] and [57] use an adaptive virtual impedance for an appropriate reactive-power sharing. In [58], the virtual inductance is dynamically adapted for achieving an adequate transient load sharing with a synchronous generator. For fault-current limiting and an improved transient stability, [59] uses an adaptive virtual impedance. [60] adapts the virtual inductor to reduce the P-Q power coupling. A dynamic virtual impedance is introduced in [61] to emulate the damping mechanism of a synchronous generator.
5. **Combinations:** [62], [63] and [16] use adaptive inertia and a virtual-impedance control strategy to improve transient stability. [64] adjusts the inertia based on the state of charge of a VSM-controlled battery to respect energy limits of the battery. In [65], the inertia constant H, cf. footnote 1 to eq. (1), is adapted whenever an active-power limit or energy limit takes a new value. H is used as a uniform value for both RoCoF directions, hence no special approach is proposed for utilizing the differing P ranges resulting from strongly asymmetric P limits like PV generation operated at the MPP and having no additional storage. An active-power limiter is presented in [66] together with [67], modifying the calculation of ΔP as well as the voltage angle of the PWM. The presented laboratory results and the explanations in [67] make clear that the active-power limiter takes around 300 ms to bring an over- or undershoot back into the limited range. This would be too slow for an application in the context of inherent instantaneous reserve.

4 Proposed Modifications of the VSM Control Scheme

This section explains modifications of the generic VSM control scheme that we propose to make its inherent behaviour as asymmetric as necessary. Thereby, the intrinsic capabilities of units such as PV plants, heat pumps, battery storage, electric vehicles, etc., can be fully utilized for asymmetric contributions to instantaneous reserve. Perspectively, sufficient positive and negative control reserves can be aggregated from all these contributions. Technical reasons for maintaining a symmetry of the total reserves do not exist.

A pseudo solution for realizing asymmetry would be to dynamically switch T_A between one large and one small value. A look at Fig. 3, where T_A is the denominator, makes clear that very small T_A values – let alone $T_\mathrm{A}=0$ – would introduce a high gain into the control loop and thus deteriorate stability. The actual modifications of the control scheme are shown in Fig. 4. Fig. 3, which has been explained in Section 3.1, is part of it at the bottom right, but T_A has been replaced by T_Amax being defined as follows. Asymmetric inertia goes along with one positive and one negative control reserve having different absolute values one of which may be 0. The corresponding two T_A values result from applying eq. (5) to both reserves. T_Amax is the larger T_A and remains unchanged in Fig. 4 when the smaller T_A becomes effective. Subsequently, it is explained how the mechanisms of Fig. 4 change the actually effective T_A value.

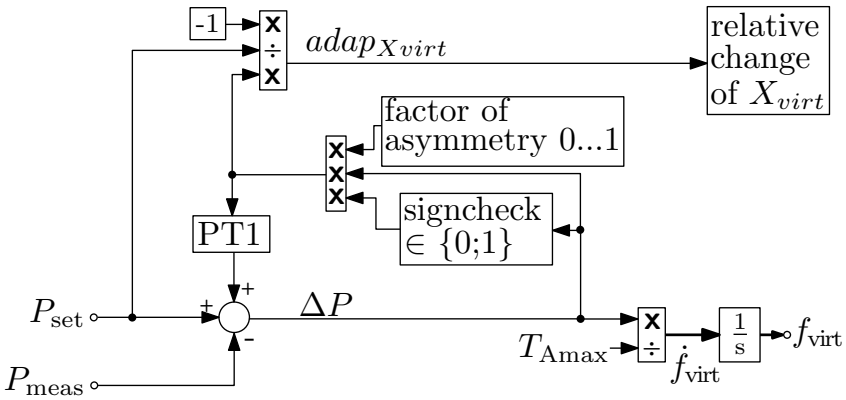

Figure 4: Modified VSM control scheme for asymmetric VSM operation. Universal VSM with ΔP calculation according to eq. (3) and $P_\mathrm{set} \leq 0$ if used for a load.

4.1 Modification of the ΔP Calculation

If the synchronous converter is to be operated asymmetrically, the block 'signcheck' in Fig. 4 checks the sign of ΔP. Its output becomes 1 if the sign corresponds to the case where a reduced T_A or $T_\mathrm{A}=0$ is assigned, and only then the triple multiplier is activated. The factor of asymmetry is explained in Section 4.3 and has a value of 1 here. The output of the multiplier, which becomes unequal 0 now, is to be understood as a correction value used to change the calculation of ΔP via a P-T1 element with a time constant $T < 2\,\mathrm{ms}$ for algebraic decoupling and stability. The thus established feedback loop realizes an actual $T_\mathrm{A}=0$ and can be thought of as a manipulation of the P setpoint until P_meas equals the original P_set.

Remark: Small enhancements to this mechanism not being in focus of this article can enforce arbitrary active-power limits. Lower and upper limits $P_{\text{lower}} \leq P_{\text{set}} \leq P_{\text{upper}}$ can be respected during unexpectedly strong RoCoFs – see the explanations to eq. (5) – while maintaining all synchronous-converter properties.

4.2 Dynamic Adaption of the Virtual Reactance

On occurrence of a voltage-angle step at the PCC, the voltage-angle difference between $\underline{V}_{\text{PCC}}$ and $\underline{V}_{\text{virt}}$ (cf. Fig. 2) jumps to a new value, causing the VSM to adjust the current through $\underline{Z}_{\text{virt}}$ accordingly, leading to a changed P_{meas}. Realizing $T_{\text{A}}=0$ or a very small T_{A} by only the mechanism shown in Section 4.1 leads to large variations of ΔP, active-power oscillations and/or a slow adaption of P_{meas} to the desired value. In order to avoid all that, the virtual reactance X_{virt} is modified – for active current only – following a relative adaption value $adap_{X\text{virt}} = -\frac{\Delta P}{P_{\text{set}}}$. $adap_{X\text{virt}} > 0$ increases X_{virt}, $adap_{X\text{virt}} < 0$ decreases it. By combining this mechanism with the feedback loop of ΔP from Section 4.1, a synchronous converter can return very quickly ($< 30\,\text{ms}$) to its original P_{set} after a large event in the grid, e.g. a system split, cf. Section 5.

4.3 Factor of Asymmetry

All cases considered in this Section 4 have in common that in one RoCoF direction the full control reserve represented by T_{Amax} shall be provided. The other RoCoF direction has $T_{\text{A}} = 0$ if the factor of asymmetry shown in Fig. 4 has the value 1. If the factor of asymmetry is set to a value < 1, the effective T_{A} for the other direction becomes $T_{\text{Amax}} \cdot (1 - \text{factor of asymmetry})$.

A typical example for this can be the charging process of an electric vehicle. Usually, the charging power is not in the middle between the maximum and minimum charging power P_{max} and P_{min}, so the control reserves have a different size in each direction of a RoCoF. By using this asymmetry factor, the different reserves can be utilized to their respective full extent. The operating principle of the asymmetry factor is that it loops back a reduced ΔP and not the full ΔP. Thereby, only part of the active-power change corresponding to the RoCoF is supressed. Numerical Example:

A charging station with synchronous converter has a working point of $|P_{\text{set}}| = 0.35\,\text{p.u.}$, with $|P_{\text{max}}| = 0.5\,\text{p.u.}$ and $P_{\text{min}} = 0\,\text{p.u.}$ Hence, the positive control reserve ($|P|$ reduction) is $0.35\,\text{p.u.}$ and the negative control reserve is $0.15\,\text{p.u.}$ Using a generic VSM control scheme without modifications would restrict the synchronous converter to having symmetric control reserves of $\pm 0.15\,\text{p.u.}$, and eq. (5) would yield $T_{\text{A}} = 3.75\,\text{s}$ if strongest RoCoFs of $\pm 2\,\text{Hz/s}$ are assumed. This would neglect the potential of the larger active-power reserve. However, utilizing the factor of asymmetry of $1 - 0.15/0.35 \approx 0.57$ would allow to associate $T_{\text{A}} = T_{\text{Amax}} = 8.75\,\text{s}$ with the positive control reserve. Doing so, the synchronous converter can make full use of both reserves.

5 Feasibility Study

For demonstrating the basic feasibility of the approach, typical applications of the asymmetric operating options according to Sections 2.1 and 2.2 were modelled and simulated. The EMT (electromagnetic transient) simulations have been carried out in Simulink/SimScape using an averaged model for the power-electronic switches. This section describes the simulations and evaluates their results.

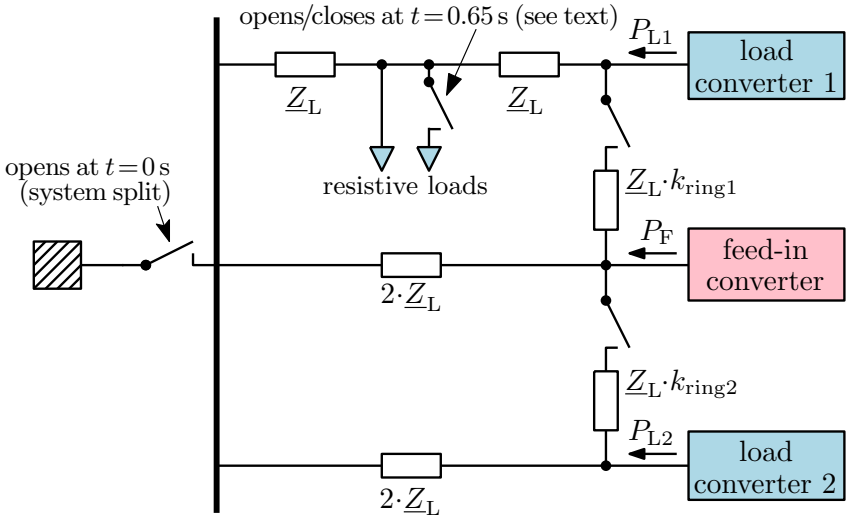

Figure 5: Grid section used in the feasibility study

All simulation settings, see below, have in common that they use the grid section in Fig. 5 with three synchronous converters, one used for feed-in and two for loads, plus a switchable resistive load. In contrast to VSM models using a $P(f)$ damping [48, p. 5] [56, pp. 581f] [58, p. 1224], the model used for designing the modifications in Section 4 and for the feasibility study is based on a generic model without immanent $P(f)$ behaviour, [3] realizing the damping via modification of the voltage angle of $\underline{V}_{PWM}$ [22, pp. 10f] [46, p. 60] [24, p. 121].
Two case studies were chosen to represent the following:

Case 1 'unidirectional': power-electronically coupled generation and load that can only reduce their P, cf. Section 2.1; see results in Fig. 6 and Fig. 7.

Case 2 'bidirectional': the situation that bidirectional but asymmetric instantaneous reserve is only contributed by two power-electronically coupled loads whereas the generation in the grid section has no inertia, cf. Section 2.2; see results in Fig. 8.

Each of the two case studies has one situation with a negative and one with a positive active-power imbalance after the system split, resulting in a negative or positive RoCoF, respectively. Variations to the simulation settings have been introduced by using different voltage levels and line lengths as seen in Table 1. Simulations for Case 1 and Case 2 have been performed with

- the voltages and line types from Table 1, to show the ability of coping with large active-power imbalances on all levels,
- the base line length and 1/10 of it, to vary the extension of the grid,

[3] If required, general or selective $P(f)$ behaviour (e.g. LFSM-O) can easily be activated.

- both rings open or one or both rings closed with $k_{\text{ring1,2}} \in \{0.1; 0.0001\}$, to vary the electrical distances between the converters.

Voltage level (kV)	0.4	20	110	**110**	400
Line type	cable NAYY 4x240SE	cable NA2XS2Y 1×500 RM it	cable N2XS2Y 1x630RM/35 it	**overhead line** **2x Al/St 435(55)**	overhead line 4x Al/St 265/35
Impedance per unit (Ω/km)	0.126+j0.080	0.068+j0.102	0.031+j0.126	**0.033+j0.260**	0.027+j0.253
base line length (km)	0.4	11.1	47.4	**47.4**	141.9

Table 1: Combinations of simulation settings chosen for the feasibility study

The simulation results that are shown in the following were conducted with unshortened 110 kV overhead lines and both rings being open. Thereby, settings have been chosen whose results are among those with the strongest undesirable effects in terms of frequency and power deviations from the ideal case and less-quick decay of oscillations. The entirety of investigated combinations of settings cover a broad range of application, so the results are significant regarding the basic feasibility of the proposed VSM control.

The simulation design is oriented at showing the pure effects of the novel approach, hence no continuously-working $P(f)$ mechanisms like primary control or LFSM-O are implemented. Each simulation starts with a system split: At $t = 0$ s, the grid section is disconnected from the interconnected grid, and the resulting active-power imbalance initiates a steep frequency slope. At $t = 0.5$ s, the frequency deviation reaches ± 1 Hz since the converter units are parameterized (see Table 2) in a way that the grid encounters a RoCoF of ± 2 Hz/s to evaluate the most critical case for a RoCoF [1, p. 3]. After additional 150 ms, in case of a negative RoCoF, a simplified one-stage UFLS mechanism (under-frequency load shedding) becomes effective, i.e. a part of the resistive load is shed 0.65 s after the system split. In case of a positive RoCoF, an additional load is connected at the same point in time to contain the frequency.

Mode	**Parameter**	**feed-in converter**	**load converter 1**	**load converter 2**
all	P_{set}	0.915 p.u.	-0.15 p.u.	-0.35 p.u.
symmetric	T_{A}	2.31 s	2.31 s	2.31 s
unidirectional inertia (Case 1)	T_{A} RoCoF up	7.2 s	0	0
	T_{A} RoCoF down	0	2.05 s	4.8 s
bidirectional inertia (Case 2)	T_{A} RoCoF up	0	2.2 s	5.8 s
	T_{A} RoCoF down	0	5.1 s	2.5 s

	P_{load} **preswitch**	P_{load} **postswitch**
case: more load than generation	0.73 p.u.	0.35 p.u.
case: more generation than load	0.1 p.u.	0.45 p.u.

Table 2: Used parameters for active-power setpoints and T_{A} in the feasibility study

Results for Case 1 'unidirectional': Fig. 6 and Fig. 7 show the frequency and the active power of exemplary simulations with unidirectionally-acting synchronous converters. For the sake of clarity, the two load converters are cumulated in these figures. Solid lines represent the unidirectionally-acting converters. For reference, dotted lines indicate results for the same grid and resistive load but with symmetrically-acting VSMs having the same power setpoints.

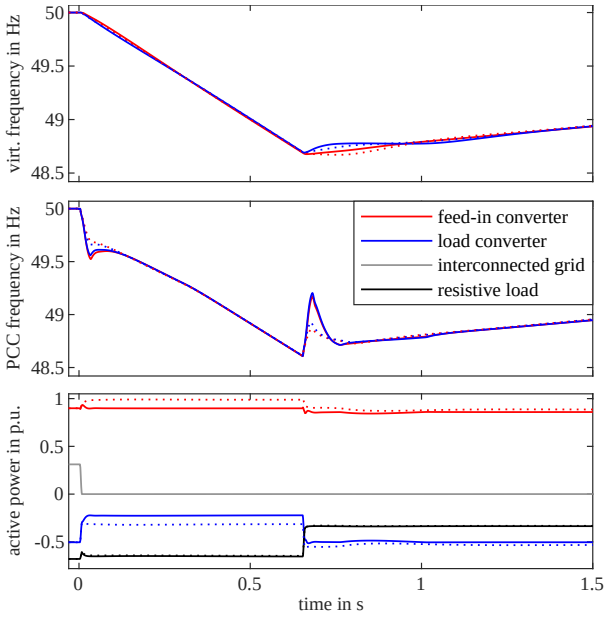

Figure 6: Virtual frequencies of the synchronous converters (top), frequencies at the PCCs (center), and active power for Case 1 having more load than generation after the system split with unidirectionally-acting VSMs (solid) and symmetrically-acting VSMs (dotted) for comparison

In the top plot of Fig. 6, the internal frequencies of the synchronous converters are shown whereas in the centre plot the PCC frequencies are shown (cf. Fig. 2). At the bottom, the active power for the feed-in converter, the accumulated load converters and the resistive load is shown. All plots of the PCC frequencies in Fig. 6 through Fig. 8 have peaks starting at the moments $t = 0\,\mathrm{s}$ and $t = 0.65\,\mathrm{s}$. These result from the way in which the frequency-measurement PLLs (phase-locked loops) track rapid voltage-angle changes – which are stronger when the mechanisms described in Section 4 set in.

Whereas there are no important differences in the frequency behaviours between the symmetrically and the unidirectionally operated VSMs, the active power behaves differently as expected. During the negative RoCoF, the feed-in converter has an effective $T_\mathrm{A} = 0$ and deviates from the reference case by not increasing its power (except for the little peak at $t = 0\,\mathrm{s}$). The load converters on the other hand decrease their power more than in the symmetric case, covering the entire power imbalance. The load is shed at $t = 0.65\,\mathrm{s}$ in order to contain the frequency. A positive RoCoF results. The active-power consumptions of the load converters return to their original values whereas the feed-in converter reduces its active power slightly. If the converters had a conventional control, the grid would have collapsed after the system split.

The deviations between the internal frequencies of the load and feed-in converters after the load shedding are caused by the change of roles between them with respect to the exertion of inertia. 300 ms after the load shedding, the frequencies cross and are converging.

Fig. 7 shows how the unidirectionally-acting synchronous converters of Case 1 cope with a positive active-power imbalance after a system split, leading to a positive RoCoF. Compared to Fig. 6 the roles are now swapped: With an effective $T_\mathrm{A} = 0$, the load converters keep their active power unchanged after the system split while the feed-in converter provides all the necessary

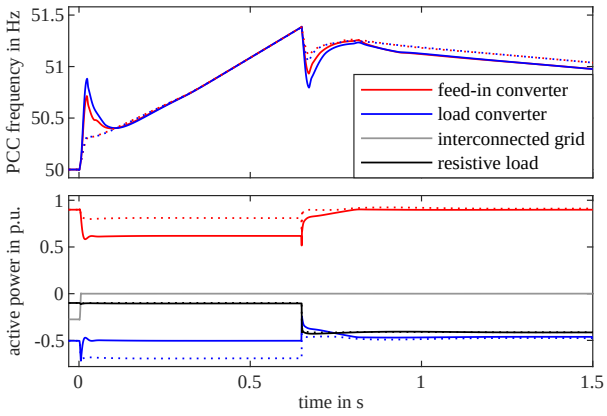

Figure 7: Frequencies at the PCCs and active power for Case 1 having more generation than load after the system split with unidirectionally-acting VSMs (solid) and symmetrically-acting VSMs (dotted) for comparison

instantaneous reserve by lowering its active power. When the consumption of the resistive load is increased to contain the frequency after 0.65 s, the RoCoF direction changes and, similar to before, the feed-in and load converters switch roles with respect to the exertion of inertia.

In Fig. 7, the peak in the active power of the load converters at the moment of the system split is stronger when compared to the corresponding peak of the feed-in converter in Fig. 6. This is due to the fact that the two load converters are cumulated and are actually two converters. Hence, the individual peaks are lower in their amplitude and not a large deviation from the ideal case.

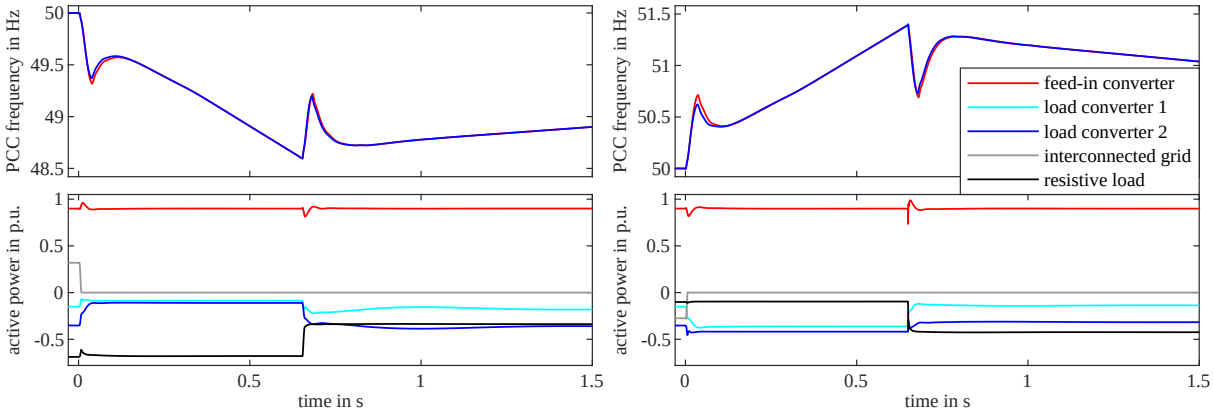

Figure 8: Frequencies at the PCCs and active power after the system split for Case 2 with a constant-power feed-in converter and bidirectionally but asymmetrically operated load VSMs. Left: more load than generation after system split. Right: more generation than load after system split.

Results for Case 2 'bidirectional': Fig. 8 shows the exemplary results for the case study with bidirectionally but asymmetrically operated load converters. The feed-in converter is set to provide an almost constant active-power output by changing the signcheck block from Fig. 4 to a constant 1 and thus suppressing active-power variations in either direction. The parameterization of the load converters is oriented at the introductory example for the use of the asymmetry factor given in Section 4.3: Load converter 1 has a setpoint of $|P_{\mathrm{set}}| = 0.15\,\mathrm{p.u.}$ and load con-

verter 2 has $|P_{\mathrm{set}}| = 0.35\,\mathrm{p.u.}$ whereas both have $P_{\mathrm{min}} = 0\,\mathrm{p.u.}$ and $|P_{\mathrm{max}}| = 0.5\,\mathrm{p.u.}$ Hence, both have a smaller reserve of 0.15 p.u. and a larger reserve of 0.35 p.u. but with different signs. On occurrence of a frequency slope, the one load converter where the larger reserve is associated with the sign of the RoCoF will use its T_{Amax}, whereas the other load converter will make its reduced T_{A} effective. Based on the ratio of the available control reserves for instantaneous reserve, the factor of asymmetry results to be $1 - \frac{0.15}{0.35} \approx 0.57$ for both load converters.

Fig. 8 shows the results for the negative power imbalance after the system split on the left side and the results for the positive power imbalance on the right side. What can be seen easily is the constant output power of the feed-in converter except the moments of the system split and the load step. Looking at the load converters, the effect of the asymmetry factor can be seen. In the results shown on the left side, the asymmetry factor is used by load converter 1. It does not decrease its power as much as load converter 2.

The opposite case for the use of the asymmetry factor can be seen on the right side: Since load converter 2 has the smaller reserve for that RoCoF direction, load converter 2 does not increase its power as much as load converter 1, which has a larger active-power reserve in that direction. After the load is switched and the direction of the RoCoF changes, the converter that exerted inertia regulary reduces its effective T_{A} whereas the converter that had its effective T_{A} reduced returns to its T_{Amax}. That becomes perceptible in each of the two active-power diagrams as a qualitative difference by comparing the beginnings and ends of the corresponding active-power graphs in a magnified view.

These results show that unidirectionally operated VSMs and bidirectionally but asymmetrically operated VSMs fulfil the expectations with respect to the provision of inherent instantaneous reserve.

6 Conclusion

A modification of a generic VSM control scheme is proposed and its working principles as well as its effects are described. Its implementation in future VSMs of feed-in inverters, different kinds of power-electronically coupled loads, and storage opens the perspective of tailoring contributions to instantaneous reserve to the characteristics and – oftentimes situation-dependent – power limitations of the different units. Thereby, tapping the full potential for contributions to instantaneous reserve by all kinds of power-electronic units gets within reach. Thus focusing on smart control, efforts for symmetric provision of instantaneous reserve can be minimized.

In order to cope with the most extreme contingencies, large portions of generation and consumption side must be enabled to contribute instantaneous reserve by – eventually strong – variations of their own active power. In the interconnected grid, participating in instantaneous reserve involves only slight active-power differences over years. Most of the corresponding slight amounts of energy can be expected to be covered by the DC-link capacitor of the converter. Large contingencies happen rarely, and even the energy drawn by a worst-case system split is way below one per mille of the energy throughput of the unit per hour. Given the short time scale, the outcome is not at all perceptible on charging/cooling/heating applications. For

the other cases, a constructive perspective is: Letting a productively used device undergo a sudden short interruption of its normal function every several years actually might be an attractive techno-economical trade-off. It is reasonable to minimize the cost of preventing blackouts, and load shedding (for tens of minutes) is one of the established measures today.

Applications in the fields of charging, cooling, and heating can easily follow power fluctuations and are the low-hanging fruits for minimizing costs and optimizing the use of resources for future instantaneous reserve. After 2030, more and longer situations are to be expected where the instantaneous reserve necessary for the most extreme cases, i.e. to avoid blackouts in large percentages of Continental Europe, can by far not be covered by synchronous machines. Co-utilizing non-dedicated units like sketched in Section 2 can save a considerable amount of capital expenditure for dedicated machinery such as powerful storages and permanently coupled synchronous condensers with inertia.

7 Outlook

In order to actually realize the potential for instantaneous reserve by power-electronically coupled loads and generation, the following is still necessary:

The dynamic X_{virt} adaption needs to be optimized using methods of control theory. Operation of synchronous converters following the design principles outlined in this paper together with conventional feed-in inverters, synchronous and induction machines as well as various kinds of power-electronic loads is to be investigated in detail. Furthermore, the control concepts presented here and investigated in simulation must be validated in a laboratory environment and subsequent field tests.

Finally, an appropriate regulatory framework must facilitate the implementation of synchronous converters featuring asymmetric contributions to instantaneous reserve by sufficient loads and renewable generators to cope with the decrease of conventional sources of instantaneous reserve expected in the future.

8 Acknowledgement

This work was supported by the German Federal Ministry for Economic Affairs and Climate Action and the Projekttraeger Juelich GmbH (PtJ) within the framework of the projects Netzregelung 2.0 (FKZ: 0350023C) and Ladeinfrastruktur 2.0 (FKZ: 0350048D). The responsibility for the content of this publication lies with the authors. This paper does not necessarily reflect the consolidated opinion of the project consortium “Netzregelung 2.0”

References

[1] ENTSO-E, “Frequency Stability Evaluation Criteria for the Synchronous Zone of Continental Europe,” ENTSO-E, Tech. Rep., 2016.

[2] M. Eremia and M. Shahidehpour, Eds., *Handbook of Electrical Power System Dynamics*. Hoboken, NJ: John Wiley & Sons, Ltd, 2013.

[3] "Netzentwicklungsplan Strom 2035 (2021), zweiter Entwurf | Übertragungsnetzbetreiber."
[4] Hg. v. Projektträger Jülich, "Forschungsroadmap Systemdienstleistungen," Brochure, Jülich, 2020.
[5] M. Braun, J. Brombach, C. Hachmann, D. Lafferte, A. Klingmann, W. Heckmann, F. Welck, D. Lohmeier, and H. Becker, "The Future of Power System Restoration: Using Distributed Energy Resources as a Force to Get Back Online," *IEEE Power and Energy Magazine*, vol. 16, no. 6, pp. 30–41, 2018.
[6] B. Xu, C. Gao, J. Zhang, J. Yang, B. Xia, and Z. He, "A Novel DC Chopper Topology for VSC-Based Offshore Wind Farm Connection," *IEEE Transactions on Power Electronics*, vol. 36, no. 3, pp. 3017–3027, 2021.
[7] J. Zhu, C. D. Booth, G. P. Adam, A. J. Roscoe, and C. G. Bright, "Inertia Emulation Control Strategy for VSC-HVDC Transmission Systems," *IEEE Transactions on Power Systems*, vol. 28, no. 2, pp. 1277–1287, 2013.
[8] E. Waffenschmidt, "Virtual inertia grid control with LED lamp driver," in *2016 International Energy and Sustainability Conference (IESC)*, 2016, pp. 1–6.
[9] J. A. Suul, S. D'Arco, and G. Guidi, "Virtual Synchronous Machine-Based Control of a Single-Phase Bi-Directional Battery Charger for Providing Vehicle-to-Grid Services," *IEEE Transactions on Industry Applications*, vol. 52, no. 4, pp. 3234–3244, 2016.
[10] I. Ibrahim, C. O'Loughlin, and T. O'Donnell, "Virtual Inertia Control of Variable Speed Heat Pumps for the Provision of Frequency Support," *Energies*, vol. 13, no. 8, 2020. [Online]. Available: https://www.mdpi.com/1996-1073/13/8/1863
[11] R. Zhang, X. Chu, W. Zhang, and Y. Liu, "Active Participation of Air Conditioners in Power System Frequency Control Considering Users' Thermal Comfort," *Energies*, vol. 8, no. 10, pp. 10 818–10 841, 2015.
[12] J. Vorwerk, U. Markovic, P. Aristidou, E. Vrettos, and G. Hug, "Modelling of variable–speed refrigeration for fast–frequency control in low–inertia systems," *IET Smart Grid*, vol. 3, no. 6, pp. 924–936, 2020.
[13] ENTSO-E, "High Penetration of Power Electronic Interfaced Power Sources," ENTSO-E, Tech. Rep., 2017.
[14] R. Shi, X. Zhang, C. Hu, H. Xu, J. Gu, and W. Cao, "Self-tuning virtual synchronous generator control for improving frequency stability in autonomous photovoltaic-diesel microgrids," *Journal of Modern Power Systems and Clean Energy*, vol. 6, no. 3, pp. 482–494, 2018.
[15] J. Han, Z. Liu, and N. Liang, "Nonlinear Adaptive Robust Control Strategy of Doubly Fed Induction Generator Based on Virtual Synchronous Generator," *IEEE Access*, vol. 8, pp. 159 887–159 896, 2020.
[16] J. Gouveia, C. L. Moreira, and J. A. P. Lopes, "Rule-based adaptive control strategy for grid-forming inverters in islanded power systems for improving frequency stability," *Electric Power Systems Research*, vol. 197, p. 107339, 2021.
[17] W. Hu, Z. Wu, X. Dou, M. Hu, and H. Song, "Dynamic Analysis and Parameters Design of the Load Virtual Synchronous Machine," in *2018 IEEE Power Energy Society General Meeting (PESGM)*, 2018, pp. 1–5.
[18] J. Guo, Y. Chen, W. Wu, X. Wang, Z. Xie, L. Xie, and Z. Shuai, "Wideband dq-Frame Impedance Modeling of Load-Side Virtual Synchronous Machine and Its Stability Analysis in Comparison With Conventional PWM Rectifier in Weak Grid," *IEEE Journal of Emerging and Selected Topics in Power Electronics*, vol. 9, no. 2, pp. 2440–2451, 2021.
[19] Y. Wang, Y. Xie, Z. Shi, and H. Ma, "A fast stable control scheme for VIENNA rectifier," in *2015 18th International Conference on Electrical Machines and Systems (ICEMS)*, 2015, pp. 355–358.
[20] J. Lee and K. Lee, "A Novel Carrier-Based PWM Method for Vienna Rectifier With a Variable Power Factor," *IEEE Transactions on Industrial Electronics*, vol. 63, no. 1, pp. 3–12, 2016.
[21] X. Yan, F. Qin, J. Jia, Z. Zhang, X. Li, and Y. Sun, "Virtual synchronous motor based-control of Vienna rectifier," *Energy Reports*, vol. 6, pp. 953–963, 2020. [Online]. Available: https://www.sciencedirect.com/science/article/pii/S2352484720315237
[22] P. Unruh, M. Nuschke, P. Strauß, and F. Welck, "Overview on Grid-Forming Inverter Control Methods," *Energies*, vol. 13, no. 10, p. 2589, 2020.
[23] D. Duckwitz, F. Welck, and C. Glöckler, "Operational behavior of the virtual synchronous machine," in *12. Fachtagung Netzregelung und Systemführung*. VDE Verlag, 2017.
[24] D. Duckwitz, "Power System Inertia: Derivation of Requirements and Comparison of Inertia Emulation Methods for Converter-Based Power Plants," Ph.D. dissertation, Universität Kassel, 2019. [Online]. Available: https://kobra.uni-kassel.de/handle/123456789/11261
[25] J. Alipoor, Y. Miura, and T. Ise, "Distributed generation grid integration using virtual synchronous generator with adoptive virtual inertia," in *2013 IEEE Energy Conversion Congress and Exposition*, 2013, pp. 4546–4552.
[26] ——, "Power System Stabilization Using Virtual Synchronous Generator With Alternating Moment of Inertia," *IEEE Journal of Emerging and Selected Topics in Power Electronics*, vol. 3, no. 2, pp. 451–458, 2015.

[27] U. Markovic, N. Früh, P. Aristidou, and G. Hug, "Interval-Based Adaptive Inertia and Damping Control of a Virtual Synchronous Machine," in *2019 IEEE Milan PowerTech*, 2019, pp. 1–6.
[28] D. Li, Q. Zhu, S. Lin, and X. Y. Bian, "A Self-Adaptive Inertia and Damping Combination Control of VSG to Support Frequency Stability," *IEEE Transactions on Energy Conversion*, vol. 32, no. 1, pp. 397–398, 2017.
[29] C. Zhang, Y. Yang, H. Miao, and X. Yuan, "An improved adaptive inertia and damping control strategy for virtual synchronous generator," in *2018 13th IEEE Conference on Industrial Electronics and Applications (ICIEA)*, 2018, pp. 322–328.
[30] W. Li, Y. Peng, H. Zhou, Y. Liu, P. Li, and Y. Wang, "Modeling and Analysis of Parallel VSGs with Consensus Control," in *2019 4th IEEE Workshop on the Electronic Grid (eGRID)*, 2019, pp. 1–8.
[31] P. Xing, X. Jia, C. Tian, Y. Mao, L. Yu, and X. Jiang, "Pre-synchronization Control Method of Virtual Synchronous Generator with Alterable Inertia," in *2019 IEEE 10th International Symposium on Power Electronics for Distributed Generation Systems (PEDG)*, 2019, pp. 142–146.
[32] D. Mengxue, L. Zhisong, X. Wei, Z. Xiaoyu, and L. Jianyu, "Research on Adaptive Control of Virtual Synchronous Generator," in *2020 IEEE 4th Information Technology, Networking, Electronic and Automation Control Conference (ITNEC)*, vol. 1, 2020, pp. 1169–1174.
[33] M. Malekpour, A. Kiyoumarsi, and M. Gholipour, "A hybrid adaptive virtual inertia controller for virtual synchronous generators," *International Transactions on Electrical Energy Systems*, vol. 31, no. 7, p. e12913, 2021.
[34] L. Huang, C. Yang, M. Song, H. Yuan, H. Xie, H. Xin, and Z. Wang, "An Adaptive Inertia Control to Improve Stability of Virtual Synchronous Machines Under Various Power Grid Strength," in *2019 IEEE Power Energy Society General Meeting (PESGM)*, 2019, pp. 1–5.
[35] U. Markovic, Z. Chu, P. Aristidou, and G. Hug, "LQR-Based Adaptive Virtual Synchronous Machine for Power Systems With High Inverter Penetration," *IEEE Transactions on Sustainable Energy*, vol. 10, no. 3, pp. 1501–1512, 2019.
[36] A. J. Marin-Hurtado, A. Escobar-Mejía, and W. J. Gil-González, "Adaptive Inertia for a Virtual Synchronous Machine Using an LQR Controller Applicable to a High-Voltage DC Terminal," in *2020 IEEE ANDESCON*, 2020, pp. 1–6.
[37] T. Li, B. Wen, and H. Wang, "A Self-Adaptive Damping Control Strategy of Virtual Synchronous Generator to Improve Frequency Stability," *Processes*, vol. 8, no. 3, 2020. [Online]. Available: https://www.mdpi.com/2227-9717/8/3/291
[38] D. Jiawei, Z. Jiangbin, and M. Zihan, "VSG Inertia and Damping Coefficient Adaptive Control," in *2020 Asia Energy and Electrical Engineering Symposium (AEEES)*, 2020, pp. 431–435.
[39] X. Wan, Y. Gan, F. Zhang, and F. Zheng, "Research on Control Strategy of Virtual Synchronous Generator Based on Self-Adaptive Inertia and Damping," in *2020 4th International Conference on HVDC (HVDC)*, 2020, pp. 1006–1012.
[40] S. Lin, L. Lin, and B. Wen, "A Voltage Control Strategy of VSG Based on Self-Adaptive Inertia Coefficient and Droop Coefficient," *Mathematical Problems in Engineering*, vol. 2021, 2021.
[41] G. Bao, H. Tan, K. Ding, M. Ma, and N. Wang, "A Novel Photovoltaic Virtual Synchronous Generator Control Technology Without Energy Storage Systems," *Energies*, vol. 12, no. 12, 2019. [Online]. Available: https://www.mdpi.com/1996-1073/12/12/2240
[42] Z. Lv, Y. Zhang, Y. Xia, and W. Wei, "Adjustable inertia implemented by bidirectional power converter in hybrid AC/DC microgrid," *IET Generation, Transmission & Distribution*, vol. 14, no. 17, pp. 3594–3603, 2020.
[43] L.-Y. Lu and C.-C. Chu, "Consensus-Based Secondary Frequency and Voltage Droop Control of Virtual Synchronous Generators for Isolated AC Micro-Grids," *IEEE Journal on Emerging and Selected Topics in Circuits and Systems*, vol. 5, no. 3, pp. 443–455, 2015.
[44] ——, "Consensus-Based Droop Control of Isolated Micro-Grids by ADMM Implementations," in *2018 IEEE Power Energy Society General Meeting (PESGM)*, 2018, p. 1.
[45] L. Chen, Y. Wang, L. Yang, Y. Si, T. Chen, and S. Mei, "Consensus control strategy with state predictor for virtual synchronous generators in isolated microgrid," in *2016 IEEE International Conference on Power System Technology (POWERCON)*, 2016, pp. 1–5.
[46] F. Welck, D. Duckwitz, and C. Gloeckler, "Influence of Virtual Impedance on Short Circuit Performance of Virtual Synchronous Machines in the 9-Bus System," in *NEIS 2017; Conference on Sustainable Energy Supply and Energy Storage Systems*, 2017, pp. 1–7.
[47] Y. Ma, F. Wang, and L. M. Tolbert, "Virtual Synchronous Generator with Limited Current – Impact on System Transient Stability and Its Mitigation," in *2020 IEEE Energy Conversion Congress and Exposition (ECCE)*, 2020, pp. 2773–2778.

[48] C.-K. Nguyen, T.-T. Nguyen, H.-J. Yoo, and H.-M. Kim, "Improving Transient Response of Power Converter in a Stand-Alone Microgrid Using Virtual Synchronous Generator," *Energies*, vol. 11, no. 1, 2018. [Online]. Available: https://www.mdpi.com/1996-1073/11/1/27

[49] Y. Wang, B. Liu, and S. Duan, "Transient Performance Comparison of Modified VSG Controlled Grid-Tied Converter," in *2019 IEEE Applied Power Electronics Conference and Exposition (APEC)*, 2019, pp. 3300–3303.

[50] ——, "Modified virtual inertia control method of VSG strategy with improved transient response and power-supporting capability," *IET Power Electronics*, vol. 12, no. 12, pp. 3178–3184, 2019.

[51] H. Wu and X. Wang, "A Mode-Adaptive Power-Angle Control Method for Transient Stability Enhancement of Virtual Synchronous Generators," *IEEE Journal of Emerging and Selected Topics in Power Electronics*, vol. 8, no. 2, pp. 1034–1049, 2020.

[52] K. M. Cheema, R. Sarmad Mahmood, M. Faizan Tahir, K. Mehmood, M. Yaqoob Javed, and A. Rehman Tariq, "Modified control of Virtual Synchronous Generator for Microgrid Stability Improvement," in *2021 International Bhurban Conference on Applied Sciences and Technologies (IBCAST)*. IEEE, 2021, pp. 673–677.

[53] M. Chen, D. Zhou, and F. Blaabjerg, "Active Power Oscillation Damping Based on Acceleration Control in Paralleled Virtual Synchronous Generators System," *IEEE Transactions on Power Electronics*, vol. 36, no. 8, pp. 9501–9510, 2021.

[54] C. Sun, S. Q. Ali, G. Joos, and F. Bouffard, "Virtual Synchronous Machine Control for Low-Inertia Power System Considering Energy Storage Limitation," in *2019 IEEE Energy Conversion Congress and Exposition (ECCE)*, 2019, pp. 6021–6028.

[55] H. Zhang, S. Kim, Q. Sun, and J. Zhou, "Distributed Adaptive Virtual Impedance Control for Accurate Reactive Power Sharing Based on Consensus Control in Microgrids," *IEEE Transactions on Smart Grid*, vol. 8, no. 4, pp. 1749–1761, 2017.

[56] H. Zhang, R. Zhang, K. Sun, and W. Feng, "Performance Improvement Strategy for Parallel-operated Virtual Synchronous Generators in Microgrids," *Journal of Power Electronics*, vol. 19, no. 2, pp. 580–590, 2019.

[57] X. Liang, C. Andalib-Bin-Karim, W. Li, M. Mitolo, and Shabbir, Md Nasmus Sakib Khan, "Adaptive Virtual Impedance-Based Reactive Power Sharing in Virtual Synchronous Generator Controlled Microgrids," *IEEE Transactions on Industry Applications*, vol. 57, no. 1, pp. 46–60, 2021.

[58] Y. Peng and X. Zhang, "Analysis and Improvement of Transient Load Sharing between Synchronous Generator and Virtual Synchronous Generator in Islanded Microgrid," in *2020 IEEE 9th International Power Electronics and Motion Control Conference (IPEMC2020-ECCE Asia)*, 2020, pp. 1224–1228.

[59] B. Rathore, S. Chakrabarti, and L. Srivastava, "A Self-Regulated Virtual Impedance control of VSG in a microgrid," *Electric Power Systems Research*, vol. 197, p. 107289, 2021. [Online]. Available: https://www.sciencedirect.com/science/article/pii/S0378779621002704

[60] T. Wen, D. Zhu, X. Zou, B. Jiang, L. Peng, and Y. Kang, "Power Coupling Mechanism Analysis and Improved Decoupling Control for Virtual Synchronous Generator," *IEEE Transactions on Power Electronics*, vol. 36, no. 3, pp. 3028–3041, 2021.

[61] L. Huang, H. Xin, H. Yuan, G. Wang, and P. Ju, "Damping Effect of Virtual Synchronous Machines Provided by a Dynamical Virtual Impedance," *IEEE Transactions on Energy Conversion*, vol. 36, no. 1, pp. 570–573, 2021.

[62] M. Ren, T. Li, K. Shi, P. Xu, and Y. Sun, "Coordinated Control Strategy of Virtual Synchronous Generator Based on Adaptive Moment of Inertia and Virtual Impedance," *IEEE Journal on Emerging and Selected Topics in Circuits and Systems*, vol. 11, no. 1, pp. 99–110, 2021.

[63] D. Zhang, H. Xu, Y. Wang, L. Chen, Y. Li, and T. Hu, "Coordinated Utilization of Adaptive Inertia Control and Virtual Impedance Regulation for Transient Performance Increase of VSG Under Different Faults," in *2021 6th Asia Conference on Power and Electrical Engineering (ACPEE)*, 2021, pp. 838–843.

[64] Y. Peng, T. Yin, M. Li, Y. Wang, D. Hu, and Z. Liu, "A Sequence Impedance Modeling of VSG With Consideration of Inner Loops Control," in *2019 4th IEEE Workshop on the Electronic Grid (eGRID)*, 2019, pp. 1–5.

[65] P. Xie, C. Yuan, Y. Guan, S. Tan, M. Li, J. C. Vasquez, and J. M. Guerrero, "Stability Analysis Considering Dual Physical Constraints of Parallel-connected Virtual Synchronous Generators forming Microgrids," in *2019 IEEE Energy Conversion Congress and Exposition (ECCE)*, 2019, pp. 2092–2098.

[66] M. Abdollahi, J. I. Candela, J. Rocabert, and R. S. M. Aguilar, "Active Power Limiter for Static Synchronous Generators in Renewable Applications," in *2018 IEEE Energy Conversion Congress and Exposition (ECCE)*, 2018, pp. 998–1004.

[67] M. Abdollahi, J. I. Candela, J. Rocabert, and M. A. Elsaharty, "Active Power Limiter for Static Synchronous Generators in Renewable Applications," *IEEE Journal of Emerging and Selected Topics in Power Electronics*, p. 1, 2020.